Desalination and Water Treatment 328 (2026) 101852

Contents lists available at ScienceDirect

Desalination and Water Treatment

journal homepage: www.sciencedirect.com/journal/desalination-and-water-treatment/

Utilizing high pH of geopolymers for activation of persulfates in aqueous phenol abatement

Mehedi Rabbil [a], Mohammad Bhuyan [a], Elijah Adesanya [a], Sérgio Botelho de Oliveira [b], Antonio Alonso [c], Tero Luukkonen [a,*]

[a] Faculty of Technology, Fiber and Particle Engineering Research Unit, University of Oulu, PO Box 4300, 90014, Finland
[b] Department of Chemistry, Universidade Federal de Goiás, Goiânia, Brazil
[c] Instituto de Física, Universidade Federal de Goiás, Goiânia, Brazil

ARTICLE INFO

Keywords:
Alkali-activated materials
Geopolymers
Peroxymonosulfate activation
Advanced oxidation processes
Wastewater treatment

ABSTRACT

Persulfates have received increasing attention in advanced oxidation processes. This study investigates a new concept for the activation of peroxydisulfate (PDS) and peroxymonosulfate (PMS) using geopolymer foams as a flow-through media supplying alkalinity. In the experiments, model solutions or real wastewater containing 10 μM phenol were distributed through geopolymer foams during which the high pH of the foams enhanced the reactive species formation. PDS achieved only maximum ~30% phenol abatement (dose 2.4 mM, pH of ~12, and empty bed of contact time of ~30 min), while PMS could achieve ~100% phenol abatement under identical conditions. The efficient phenol abatement was due to the high pH of geopolymer (in the range of 8–12) while PMS alone, without pH increase, could reach only max. ~20% phenol abatement and geopolymer foam alone max. ~16% phenol abatement, likely due to adsorption. In municipal tertiary wastewater spiked with phenol, ~98% phenol abatement was achieved using the 1.2 mM dose of PMS when treating 10 bed volumes of water. In a longer experiment (72 bed volumes), a decline in abatement was observed from ~97% to ~50% as pH decreased from 11.9 to 7.3 after 48 bed volumes of treated water. Radical scavenging experiments indicated that singlet oxygen ($^1O_2$) is the most important reactive species in the geopolymer-PMS system. Also, electron paramagnetic resonance (EPR) spectroscopy measurements were conducted but they faced challenges at highly alkaline conditions possibly due to spin trap decomposition. Overall, geopolymer foam effectively activated PMS, offering a promising and easy-to-set-up advanced oxidation process not requiring expensive or toxic metals as catalysts.

1. Introduction

Geopolymers are amorphous or nanocrystalline aluminosilicates prepared of precursors (e.g., metakaolin) and alkaline solutions (called alkali activators, e.g., sodium silicate) [1]. Over the past decade, geopolymers have been studied for several wastewater treatment applications (e.g., adsorbents, filtration media, and catalyst supports) due to their ion-exchange capacity, adaptable pore structure, and ceramic-like properties [2]. In those studies, geopolymers are often used as foams which are produced for example with hydrogen peroxide and surfactants that stabilize gas bubbles during hardening, creating a porous network.

One feature of geopolymers is their residual alkalinity (i.e., their pore solution, containing residues of the alkali activator, has pH of ~13) which causes OH^- ions to slowly diffuse into surrounding water [3]. This sustained release of alkalinity from geopolymers has been utilized in applications that require passive pH increase (i.e., without continuous dosing of chemicals). For instance, in anaerobic digestion of organic matter (where the formation of fatty acids decreases pH), geopolymer granules have been tested to maintain pH between 6.5 and 7.2 to improve methane production [4,5]. In acid mine drainage treatment, they have been studied as permeable reactive barriers to increase pH and simultaneously remove toxic metals [6]. Another, yet unexplored, application for the residual alkalinity could be the activation (i.e., enhancing the formation of reactive radicals) of peroxydisulfate (PDS, $S_2O_8^{2-}$) and peroxymonosulfate (PMS, HSO_5^-) which are widely studied oxidants in advanced oxidation processes (AOPs) [7,8]. Geopolymer

* Corresponding author.
E-mail address: tero.luukkonen@oulu.fi (T. Luukkonen).

https://doi.org/10.1016/j.dwt.2026.101852
Received 24 April 2026; Received in revised form 25 June 2026; Accepted 30 June 2026
Available online 3 July 2026

foams may offer several practical advantages as a medium for this application. Its sustained alkalinity release maintains stable pH without continuous chemical dosing. In a flow-through configuration, the foam remains fixed within the column and thus not requiring separation from the treated water. Furthermore, unlike transition metal-based activators, geopolymer foam is entirely metal-free, avoiding secondary contamination from leached metals. As geopolymers are prepared of commonly available raw materials, such as metakaolin and sodium silicate, they could be cost-effective in some water treatment scenarios.

Persulfates can be activated by heat, radiation, alkaline conditions, transition metals, or carbonaceous materials [8]. Without activation, persulfates react only slowly with organic contaminants [9]. Alkaline activation (pH > 9) is considered a simple approach for persulfate activation [8,9]. When alkaline conditions are used, the interaction of persulfates with hydroxide ions (OH^-) transforms the AOP from $SO_4^{\bullet-}$-dominated to •OH-dominated [10,11]. This results effective abatement of micropollutants compared to other persulfate activation mechanisms since •OH is less selective than $SO_4^{\bullet-}$ but this also increases consumption of persulfate [8,9]. The dominant oxidant species in alkaline activation depends whether PMS or PDS is used [7,12]. In the case of PDS, two sequential reactions occur: OH^- initiates PDS hydrolysis, forming hydroperoxide anions (HO_2^-), which then reduce additional PDS to sulfate radical ($SO_4^{\bullet-}$) which can form •OH at highly alkaline conditions (pH > 12) [11,13]. In the case of PMS, alkaline conditions cause nucleophilic attack of deprotonated PMS (SO_5^{2-}) to the peroxide oxygen of PMS (HSO_5^-), resulting self-decay of PMS and singlet oxygen ($^1O_2$) production [12,14]. It should be noted that the effect of pH on PMS activation depends strongly on the activation method. In catalyst-based systems, increasing the alkalinity can in some cases lower PMS activation and degradation performance, for example through precipitation of dissolved metal catalysts at high pH [15,16]. In contrast, the present approach does not rely on a catalyst but instead uses the residual alkalinity of the geopolymer itself as the activator, where the elevated pH is the intended driver of base activation.

The revised Urban Wastewater Treatment Directive (2024/3019) of European Union will require quaternary treatment at large wastewater treatment plants (population equivalent ≥ 150,000) starting from 2033 to achieve at least 80% abatement for at least six out of the thirteen micropollutant indicators [17]. In Switzerland, where similar legislation has been in place since 2016 [18], activated carbon or ozonation are recommended as the treatment options [19]. However, persulfate-based AOPs could be one option to address the need to remove micropollutants in situations where increasing water pH is feasible. The reactive species formed in persulfate-based AOPs have been shown to be capable of abating micropollutants, for example steroid estrogens, antibiotics, and phenol [20]. However, AOP-based treatment may not result in complete mineralization of micropollutants. Transformation products such as benzoquinone have been identified in PMS-based phenol oxidation under alkaline conditions [21], and assessing of their potential toxicity and environmental fate is important for practical applications.

In the present study, high pH of geopolymers is used to activate PDS and PMS to abate phenol as a model compound from aqueous solutions and spiked municipal tertiary wastewater. The objectives of this study were to: (i) evaluate metakaolin geopolymer foam as an activator for persulfate-based AOPs in a flow-through set-up, (ii) determine the optimum conditions (e.g., pH and type of persulfate) and effect of the individual contributions of persulfates, geopolymer, and pH conditions with control experiments, and (iii) identify the dominant reactive species.

2. Materials and methods

2.1. Geopolymer foam preparation

Metakaolin (MetaMax, BASF, Germany) was used as the aluminosilicate precursor. Oxide composition of metakaolin is presented in Table S1 (supporting information). The composition of the alkali activator solution and the mixing ratios of the raw materials were selected based on earlier literature [22,23]. The alkali activator for metakaolin consisted of 87 wt% sodium silicate solution ($SiO_2 \approx 27$ wt%, $Na_2O \approx 8$ wt%; Merck, Germany) and 13 wt% sodium hydroxide (98.7%, VWR, Sweden). The precursor was mixed with the alkali-activator solution in a weight ratio of 1.00:1.36 (total weight of 196.2 g) with the addition of 3.2 mL hydrogen peroxide (H_2O_2, 30% w/v; VWR, Belgium) and 187 μL Triton X−100 (100% solution; VWR, France), then poured into a plastic column mold (99 mm in height and 44 mm in diameter) for curing at 22 °C. The geopolymer preparation is shown in Fig. S1 (supporting information). Further details of the reagents and materials are provided in Table S2 (supporting information).

2.2. Geopolymer characterization

The materials were characterized using X-ray fluorescence (XRF), X-ray diffraction (XRD), field-emission scanning electron microscopy combined with energy-dispersive X-ray spectroscopy (FE-SEM-EDS), high-resolution transmission electron microscopy (HR-TEM), and selected area electron diffraction (SAED) with energy-dispersive X-ray spectroscopy (EDX) analyses. Detailed information on the characterization methods is provided in Text S1 (supporting information).

2.3. Analysis of persulfate and phenol concentrations

The concentrations of PDS and PMS in the oxidation experiments were measured using a UV-Vis spectrophotometer (UV−6300, VWR) following procedures reported in the earlier literature [24]. Phenol concentration was detected using liquid chromatography-mass spectrometry (LC-MS). Analyses were conducted using a Waters ACQUITY Ultra Performance Liquid Chromatography system coupled to a Q Exactive Plus mass spectrometer (Thermo Fisher Scientific). More detailed analytical methods for persulfate and phenol concentration determination are provided in Text S2 (supporting information).

2.4. Phenol abatement experiments

Phenol abatement experiments were performed using a flow-through column (99 mm height, 44 mm diameter, filled with geopolymer foam) set-up in which phenol solution or tertiary wastewater spiked with phenol (in both cases, 10 μM phenol concentration) dosed with 0.6–4.8 mM PMS or PDS was passed through the foam using a peristaltic pump at a flow rate of 300 mL h^{-1} (i.e., ~2 bed volumes [BV] per hour), corresponding to an empty bed contact time of ~30 min. To stop the oxidation reaction after sampling, pH of the sampled water (10 mL) was decreased to acidic range by adding 0.2 mL of 0.1 M nitric acid (Merck, Germany) and 50 μL of 0.1 M sodium thiosulfate pentahydrate (Merck, Germany) to quench any remaining persulfate, similarly as in [25]. Tertiary wastewater samples were collected from the Taskila wastewater treatment plant, Oulu, Finland (characterization provided in Table S3, supporting information).

To investigate the individual contributions of persulfates, geopolymer, and pH adjusted with NaOH to phenol abatement, control experiments were performed. To determine the individual contribution of PMS, 0.6–2.4 mM concentrations were added to a 10 μM phenol solution prepared in ultrapure water, mixed for 30 min with magnetic stirrer, and sampled as above for phenol concentration analysis. To determine the individual effect of pH, NaOH was used to adjust the pH of 10 μM phenol solution to 6–12 in the presence of PMS (0.6–2.4 mM), and samples were collected after 30 min reaction time for phenol analysis. Finally, the individual effect of geopolymer foam for phenol abatement (i.e., via adsorption) was determined by distributing 10 μM phenol solution through the geopolymer foam without PMS with empty bed contact time (EBCT) of 30 min (flow rate 300 mL h^{-1}). Total organic carbon (TOC) concentration was detected during the oxidation

experiments to determine whether mineralization of phenol took place (i.e., conversion to CO_2 and H_2O). TOC was detected using a TOC-L analyzer (Shimadzu).

Radical scavenger experiments were conducted in the flow-through column for a duration of 1 h and EBCT of 30 min using the following chemicals as scavengers: tert-butanol (TBA, 100 mM) for •OH, isopropanol (IPA, 100 mM) combined with furfuryl alcohol (FFA, 1 mM) for •OH, SO_4•$^-$, and $^1O_2$, and FFA (1 mM) alone for $^1O_2$. In addition, electron paramagnetic resonance (EPR) was used to identify the predominant reactive species formed in the PMS (pH 6–12) and PDS (pH 11–12) systems in the presence of geopolymer. The samples consisted of 40 μL aqueous solutions containing (2.4 mM-PDS or 1.2 mM-PMS) oxidant and (10 g L^{-1}) geopolymer powder, adjusted to the target pH values. Three experimental conditions were used to detect specific reactive species: 1) SO_4•$^-$, and •OH were trapped using 50 mM 5,5-dimethyl−1-pyrroline-N-oxide (DMPO), 2) an 80:20 mixture of ethylene glycol and water with 50 mM DMPO was used to detect superoxide anion (O_2•$^-$) formation, and 3) $^1O_2$ was detected using 50 mM 2,2,6,6-tetramethyl−4-piperidone (TEMP; 95%) in water. The observed EPR signals for DMPO were assigned to DMPO/•OH ($a_N = a_H = 14.9$ G), DMPO/SO_4•$^-$ ($a_N = 13.5$ G, $a_H = 2.7$ G; $a_{H\gamma1} = 1.3$ G; $a_{H\gamma2} = 0.9$ G) [26], and DMPO/O_2•$^-$ ($a_N = 13.0$ G, $a_{H\beta} = 9.8$ G and $a_{H\gamma} = 1.5$ G) [27]. Ethylene glycol and water were used as solvents for DMPO/O_2•$^-$ to prevent the rapid dismutation of O_2•$^-$ to hydrogen peroxide and molecular oxygen [28,29]. TEMP detects singlet oxygen ($^1O_2$) through the formation of TEMPO (via TEMP/$^1O_2$; $a_N = 16.1$ G) [50]. More details of the EPR analysis are provided in Text S3 (supporting information).

3. Results and discussion

3.1. Comparison of PMS and PDS when combined with geopolymer

PMS (0.6–2.4 mM) and PDS (1.2–4.8 mM) were compared as oxidizers when combined with geopolymer for phenol abatement (Fig. 1a and b). During the 5-h experiment, pH decreased from the initial value of ~12.30 to ~10.0 for PMS, and from ~12.30 to ~11.6 for PDS. PMS achieved clearly better performance (up to ~100%) than PDS (up to ~30%). Similar behavior has been reported earlier, where PDS 20 mM achieved only 41% bisphenol A removal (from initial concentration of 5 mg L^{-1}, equivalent to 21.1 μM) at pH 11 with a low pseudo-first-order rate constant ($k = 0.0035$ min^{-1}) [30]. The PDS decomposition (> 90%) (Fig. S2), indicated that PDS did not produce efficiently radicals for phenol abatement even though it was largely decomposed over the contact with the geopolymer foam. To allow a more direct comparison between the two oxidants, phenol abatement was normalized to the amount of oxidant consumed. PMS achieved approximately 39–42 μmol of phenol abated per mmol of oxidant decomposed, whereas PDS achieved only about 0.1–1.0 μmol per mmol, indicating that PMS used the

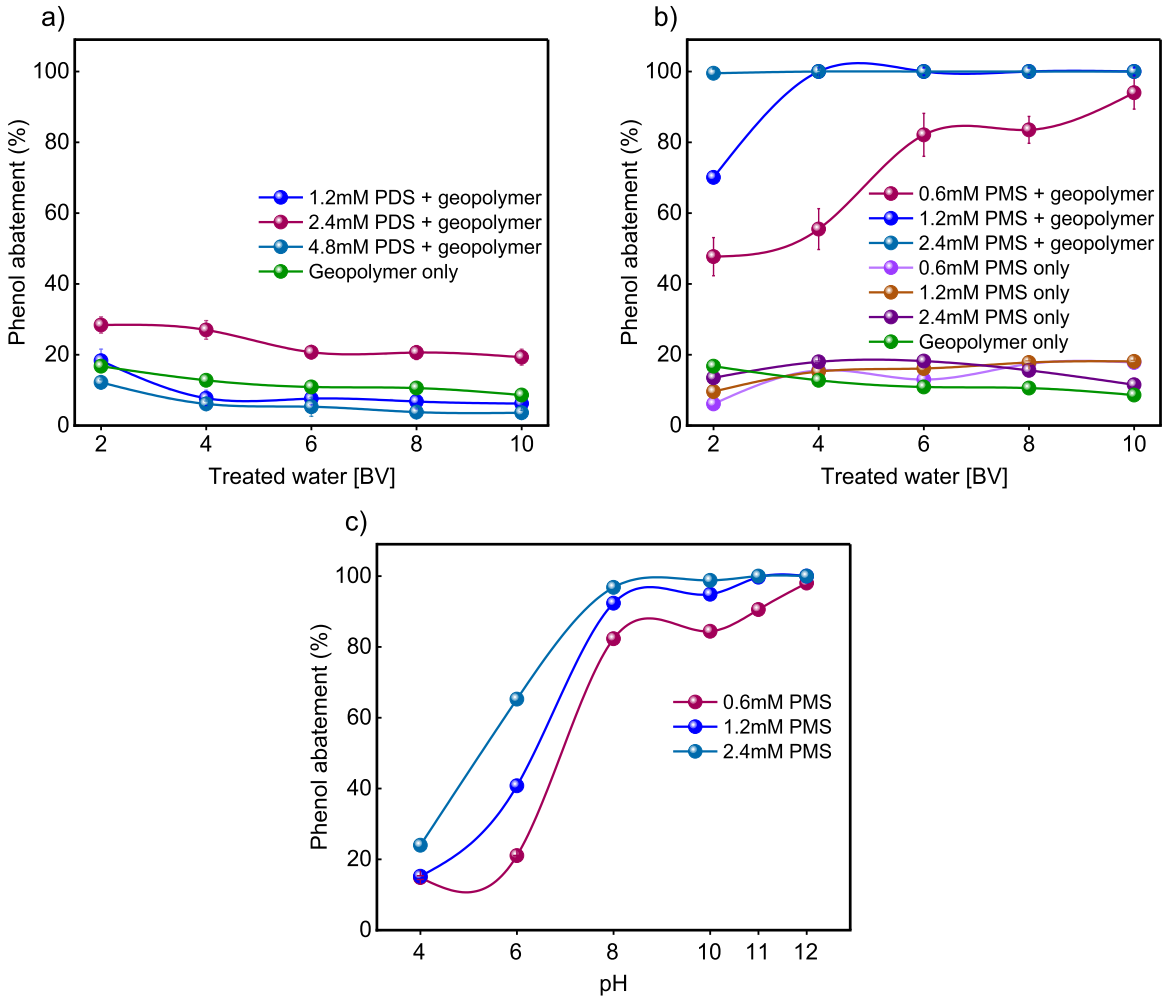

Fig. 1. Phenol abatement by (a) PDS combined with geopolymer and geopolymer alone; (b) PMS combined with geopolymer, geopolymer alone, and PMS alone; and (c) control experiment with PMS at different initial pH without geopolymer (pH decreased by ~0.10–0.40 units during the experiment). Experimental conditions: [phenol] = 10 μM, [PDS] = 1.2–4.8 mM, [PMS] = 0.6–2.4 mM, empty bed of contact time (EBCT): ~30 min (the reaction of 30 min was used for the experiments with PMS alone), 10 bed volumes (BV) treated water at 300 mL h^{-1} (5 h total), pH in a) and b) were 10–12 (those experiment with persulfates + geopolymers).

oxidant approximately 40 times more efficiently. Qi et al. [12] reported that alkaline-activated PMS at 1.0 mM concentration (pH ≈ 9.8) achieved ~90% decolorization of acid orange 7 (0.1 mM), while PDS at 1.0 mM concentration yielded negligible removal (~0%) after 60 min reaction time, confirming the differences observed in the present study [31]. Phenol abatement progressively increased as more water was treated across all PMS doses (0.6–2.4 mM), with higher PMS concentrations achieving complete abatement already at the beginning of the experiment (Fig. 1b). The reason for this increasing trend could be that initially the pH (~12.3) was too high, causing PMS deprotonation and radical scavenging.

Geopolymer alone showed only limited phenol abatement (< 20%, Fig. 1), likely mainly via adsorption. When PMS was used alone as an oxidizer (pH of ~3.30), it achieved < 20% phenol abatement, consistent with prior reports [32,33]. When PMS activation was studied at different pH without geopolymer (Fig. 1c), it was observed that pH should be > 8 to achieve high phenol abatement (> 80%), which is consistent with previous studies [34]. Thus, theses control experiments indicate that the primary mechanism of PMS activation was by the bulk solution alkalinity, rather than involvement of the geopolymer surface.

3.2. Experiments with municipal wastewater

Municipal wastewater was spiked with phenol, and two experiments were performed (10 and 72 bed volumes of treated water (Fig. 2). In both experiments, initial phenol abatement during the first treated bed volumes was between 40–60%, again likely due to too high pH (~12). However, it increased to near 100% and remained at that level up to 10–12 treated bed volumes of water (pH of ~10.2 during this time). After that, the longer experiment still had ≥ 80% removal until 48 treated bed volumes of water (pH remained at ≈ 8.75). Subsequently, the phenol abatement decreased clearly due to geopolymer foam alkalinity depletion (column effluent pH being ≈ 7.27). Under neutral conditions, PMS predominantly exists as HSO_5^- and thus SO_5^{2-} is not available for nucleophilic attack which is required for $^1O_2$ generation [7, 35,36]. This agrees with the optimal PMS activation occurring at pH 9–11 (Fig. 2). No mineralization of phenol was observed based on the TOC results (Table. S4).

3.3. Characterization of geopolymer after use in oxidation process

To examine potential changes in surface morphology, geopolymer foam was characterized before and after treatment the treatment of 72 BV (≈ 7.2 L) of wastewater using HR-TEM and SEM (Fig. 3). Prior to use, the SEM micrographs (Fig. 3a) revealed a smooth morphology containing layer-like structures which are likely unreacted metakaolin. After using the foam in wastewater treatment (Fig. 3d), EDS analysis and elemental mapping confirmed that the particulate matter on the surface was from geopolymer itself (Fig. S3), rather than organic or other matter accumulated from wastewater. Thus, as the wastewater experiment was rather short, no surface fouling or any microstructural damage was observed. This also suggests that geopolymer surface can withstand the oxidative conditions introduced by PMS.

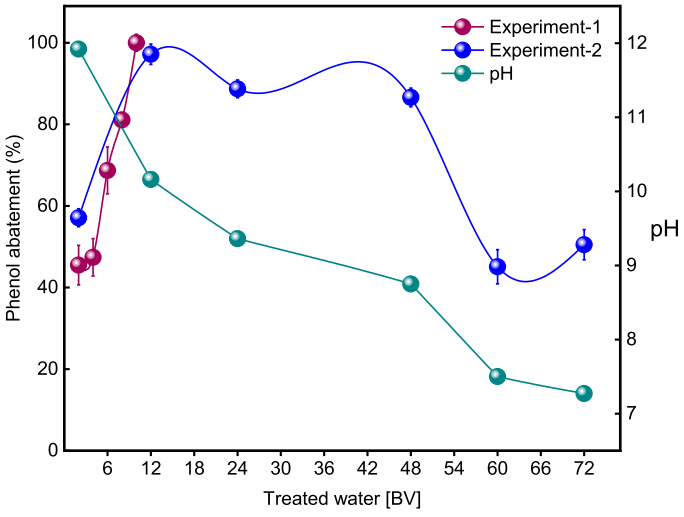

Fig. 2. Phenol abatement in spiked tertiary municipal wastewater using the geopolymer-PMS system. Experimental conditions: [phenol] = 10 μM, [PMS] = 1.2 mM, EBCT: ~30 min, flowrate ~300 mL h^{-1} , duration of the experiment 5 h (experiment 1) or 36 h (experiment 2).

The selected area electron diffraction (SAED) patterns of the unused geopolymer foams (Fig. 3b), displayed diffuse halo rings, consistent with amorphous structures of geopolymers. After the longer wastewater experiment (i.e., experiment 2 in Fig. 2), clearer electron diffraction patterns could be observed (Fig. 3e), indicating increased nanostructural ordering. The TEM image of the geopolymer before use (Fig. 3c) revealed an aggregated structure nano participles forming large clusters which is typical for geopolymers. After using geopolymer in wastewater treatment (Fig. 3f), no clear difference can be observed. EDS analysis indicated a slight increase in the Si/Al atom ratio (from 3.15 to 3.36; Fig. S4). Overall, these observations suggest that geopolymer matrix maintained structural integrity during the treatment of 72 BV of wastewater. X-ray diffraction (XRD) analyses (Fig. S5) indicated that the amorphous structure of geopolymer was preserved, and no new crystalline phases were formed during the oxidation experiment.

Visual inspection after the long-term experiment confirmed that the geopolymer foam remained intact with no visible damage, and only surface deposits from wastewater suspended solids were observed (Fig. S6). The compressive strength of the same metakaolin-based foam composition has been previously reported as 0.67 MPa with no microstructural changes after long-term flow-through use [37,38], and the flow rate remained stable throughout the present experiments. The service life of the foam is limited by its residual alkalinity, as phenol abatement declined when pH fell below 7.5.

3.4. Identification and contribution of reactive species

Electron paramagnetic resonance (EPR) characterization and radical scavenging experiments are widely used to identify the dominant reactive species roles in AOPs systems [39–41]. Recent studies indicate, however, that these methods can yield uncertain results due to non-selective reactions and competing reaction pathways, complicating identification of dominant reactive species [8,42]. This limitation has been critically discussed in the context of persulfate-based systems, where ambiguous radical assignments remain a recognized challenge [43,44].

In this study, IPA and FFA were added together to quench •OH, $SO_4^{\bullet-}$, and $^1O_2$ [45], FFA alone was used to quench $^1O_2$ [46], and TBA scavenged •OH [47]. The corresponding second-order rate constant for the reactions between the scavengers and reactive species are $k_{\bullet OH} = 6 \times 10^8\ M^{-1}\ s^{-1}$ for TBA [48]; $k_{\bullet OH} = 1.9 \times 10^9\ M^{-1}\ s^{-1}$ [48], $k_{SO_4^{\bullet-}} = 8.2 \times 10^7\ M^{-1}\ s^{-1}$ [49], and $k_{^1O_2} = 3.48 \times 10^3\ M^{-1}\ s^{-1}$ for IPA [50]; $k_{\bullet OH} = 1.5 \times 10^{10}\ M^{-1}\ s^{-1}$ [48], $k_{SO_4^{\bullet-}} = 1.3 \times 10^{10}\ M^{-1}\ s^{-1}$ [51], and $k_{^1O_2} = 1.2 \times 10^8\ M^{-1}\ s^{-1}$ [52] for FFA. It should be noted that FFA is not fully selective for $^1O_2$, as it also reacts rapidly with •OH, and $SO_4^{\bullet-}$ in persulfate-based systems [51].

The combined IPA and FFA addition markedly suppressed phenol abatement (Fig. 4a), indicating that at least one of •OH, $SO_4^{\bullet-}$, or $^1O_2$ has an important contribution for the abatement. FFA alone caused approximately similar suppression as IPA and FFA while TBA did not hinder abatement as much. Thus, the importance of the reactive species appears to be $^1O_2$ > •OH > $SO_4^{\bullet-}$ which is in agreement with the previous literature stating that alkaline conditions make the oxidation $^1O_2$/•OH-dominated instead of $SO_4^{\bullet-}$-dominated [44], and with studies identifying $^1O_2$ as the principal reactive species in other PMS-based

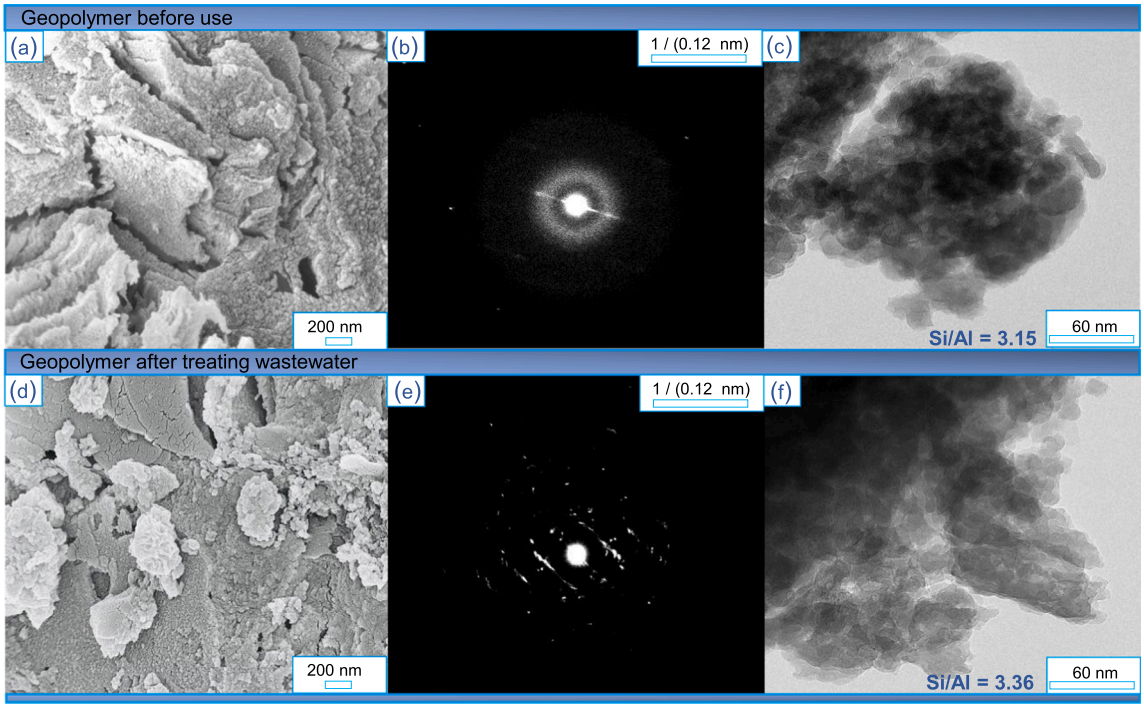

Fig. 3. HR-TEM (c, f), SEM (a, d), and SAED pattern (b, e) characterization of geopolymer before and after municipal wastewater experiment (72 BV of treated wastewater).

systems [53,54]. The pH during the scavenger experiment was 11.02–11.78.

To further confirm the reactive species in the geopolymer–PMS system, EPR measurements were conducted at pH 6–12 using DMPO to detect DMPO/•OH and DMPO/SO_4•$^-$, DMPO/O_2•$^-$, and TEMPO for $^1O_2$ ($^1O_2$ via TEMP-$^1O_2$) adducts. DMPO/•OH and DMPO/SO_4•$^-$ signals are shown in Fig. 4b. The EPR signal intensities of •OH species decreased progressively as pH increased from pH 6–12. This can be also due to an analytical artefact (spin trap degradation at elevated pH). DMPO/SO_4•$^-$ adduct signal remained low across the entire pH range (6–12) with no discernible variation (Fig. 4b) but this could be again attributable an analytical artefact which the limited trapping efficiency of DMPO for SO_4•$^-$ ($k = 2.7 \times 10^{-2}$ M^{-1} s^{-1}) and rapid conversion of DMPO/SO_4•$^-$ to DMPO/•OH via nucleophilic addition [55,56], rather than an absence of sulfate radical generation. Indeed, scavenger experiments provided more definitive evidence about $^1O_2$/•OH as the dominant reactive species in the geopolymer–PMS system, with SO_4•$^-$ having a minor role.

As shown in Fig. 4c, no DMPO/O_2•$^-$ adduct signal did not appear, instead, DMPO/•OH and methyl radical (DMPO/•CH_3) adduct signals (aN = 15.6 G, aH = 22.3 G; [57]) emerged, consistent with the rapid scavenging of •OH by DMSO to form •CH_3 ($k_{•OH,\ DMSO} = 4.5–7.1 \times 10^9$ $M^{-1}s^{-1}$) [58]. When using DMSO solvent instead of ethylene glycol (EG), a very weak DMPO/O_2•$^-$ adduct signal was observed (EPR spectrum not shown). This result suggests that the conversion of the superoxide anion to other radical species such as the hydroxyl radical may be very rapid [59]. For $^1O_2$ detection, TEMP was used to form the stable TEMPO radical (Fig. 4d). A weak background TEMPO signal, attributable to trace impurities in the TEMP reagent, was present at all pH values. From pH 6–12, TEMPO signal intensity declined gradually and then more sharply, indicating that $^1O_2$ formation decreases under alkaline conditions. However, the FFA scavenger results, which showed similar inhibition to IPA + FFA, suggest that $^1O_2$ plays an important role in phenol abatement. The decreasing TEMPO signal at higher pH value may therefore reflect analytical artefact limitation due to spin trap degradation rather than negligible $^1O_2$ involvement. This significant $^1O_2$ contribution likely reflects HSO_5^-/SO_5^{2-} self-decomposition or secondary reactions between O_2•$^-$ and •OH at high pH [7,60], suggesting that $^1O_2$ plays an important role.

In geopolymer foam, the pore solution is highly alkaline and thus releases continuously OH^- ions. At pH > 11.0 (i.e., the conditions introduced by geopolymer), the combined scavenger and EPR evidence indicated that $^1O_2$/•OH are the dominant reactive species governing phenol abatement in the geopolymer-PMS system.

4. Conclusions

This study investigated the activation of PDS and PMS by high pH introduced by geopolymer foam for phenol abatement. PMS outperformed PDS under alkaline conditions (pH 8–12), achieving complete phenol abatement at pH of around 10 while geopolymer or PMS alone showed low performance and thus confirming synergistic effect. The geopolymer-PMS system could treat ~48 bed volumes of phenol-spiked municipal wastewater with ≥ 80% abatement (the removal limit of indicator micropollutants in the updated Urban Wastewater Directive of the EU). After this, alkalinity depletion of geopolymer (i.e., effluent pH < 7.3) caused performance to decrease. No mineralization of phenol occurred based on the TOC analyses. $^1O_2$/•OH appeared to dominate the oxidation process under high alkalinity (pH ≥ 11), while SO_4•$^-$ had only a minor role according to scavenger experiments and EPR spectroscopy. It should be noted though that EPR measurement had issues with high alkalinity possibly due to the spin trap decomposition and thus its results are not fully consistent. Thus, it appears that geopolymer-activated PMS AOP follows the conventional alkaline activation mechanism where $^1O_2$ and •OH dominate instead of SO_4•$^-$. From the practical perspective, the geopolymer-PMS system appears as a potentially useful AOP for situations where its limited lifetime (max. ~48 BV treated water) and alkaline effluent are acceptable. However, future work should examine the oxidation kinetics, transformation products, the applicability of this system to other contaminants, and cost comparison of direct alkaline dosing (e.g., using NaOH) with geopolymer foam.

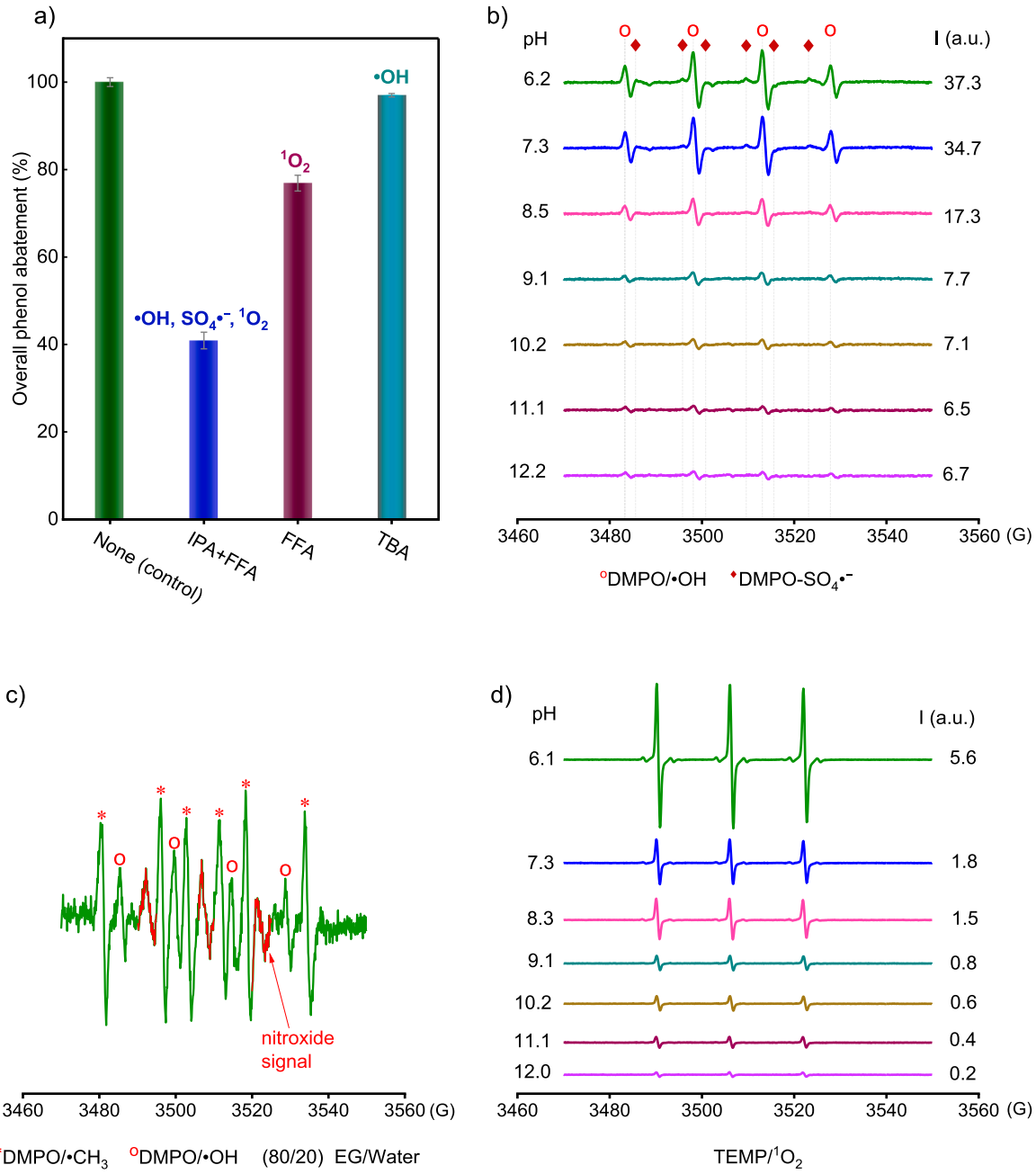

Fig. 4. (a) Effects of radical scavengers on cumulative phenol abatement over the treatment of 2 BV of synthetic phenol solution (conditions: [phenol] = 10 μM, [PMS] =1.2 mM, EBCT: ~30 min, treated water volume: 2 BV, flow rate: 300 mL h^{-1}, pH = 11.02–11.78), (b-d) EPR spectrum of radical adducts in the geopolymer-PMS system: [PMS] = 1.2 mM, geopolymer = 10 g L^{-1}, reaction time = 20 min. In panel (c), unpurified DMPO (50 mM) in an 80:20 ethylene glycol: water mixture at pH 6.1 was used. Due to the impurity of the DMPO, the nitroxide signal (red resonance lines) appeared along with signals of the DMPO/•OH and DMPO/•CH_3 adducts. Magnetic field (G) plotted on the x-axis, while relative signal intensities in arbitrary units (a.u.) appear on the y-axis.

CRediT authorship contribution statement

Mehedi Rabbil: Writing – review & editing, Writing – original draft, Methodology, Investigation, Conceptualization. **Mohammad Bhuyan:** Writing – review & editing, Validation, Methodology, Investigation. **Elijah Adesanya:** Writing – review & editing, Validation, Supervision, Methodology, Investigation. **Sérgio Botelho de Oliveira:** Writing – review & editing, Software, Investigation. **Antonio Alonso:** Writing – review & editing, Software, Methodology, Investigation. **Tero Luukkonen:** Writing – review & editing, Supervision, Methodology, Investigation, Funding acquisition, Conceptualization.

Declaration of Competing Interest

The authors declare that they have no known competing financial interests or personal relationships that could have appeared to influence the work reported in this paper.

Acknowledgements

This work was financially supported by Maa-ja vesitekniikan tukiry (grants #4886 and #5091). Assoc. Prof. Tero Luukkonen and the Fibre and Particle Engineering Research Unit are gratefully acknowledged for partial financial support. Part of the work was conducted with the

support of the Centre for Material Analysis and Biocenter Oulu, University of Oulu, Finland. The authors thank Ulrich Bergman, Anu Myllymäki, Hannele Härkman, and Senthil Thangaraj for assistance with phenol analysis at Biocenter Oulu. Markus Väyrynen and Mikko Häkkinen are acknowledged for TOC analysis. The authors also thank Akram Hossain for support with persulfate analysis. Sami Saukko, Roya Khalili, Pasi Juntunen, and Tapio Soukka are acknowledged for support with TEM and FE-SEM-EDS analysis. Monazza Khatun is gratefully acknowledged for assistance with figure preparation. Elisa Wirkkala, Jarno Karvonen, and Jani Österlund, together with the laboratory technicians of the Fibre and Particle Engineering Research Unit, are gratefully acknowledged for their technical support. Assoc. Prof. Satu Ojala and Shreenandan Sahoo are gratefully acknowledged for assistance with Raman spectral and XRD analysis. Sajad Ahmadi and Jennyffer Martinez Quimbayo are gratefully acknowledged for their valuable support and assistance with EPR measurements.

Appendix A. Supporting information

Supplementary data associated with this article can be found in the online version at doi:10.1016/j.dwt.2026.101852.

Data availability

Data will be made available on request.

References

[1] Luukkonen T, Heponiemi A, Runtti H, Pesonen J, Yliniemi J, Lassi U. Application of alkali-activated materials for water and wastewater treatment: a review. Rev Environ Sci Biotechnol 2019;18:271–97. https://doi.org/10.1007/s11157-019-09494-0.

[2] Della Rocca DG, Peralta RM, Peralta RA, Rodríguez-Castellón E, De Fatima Peralta Muniz Moreira R. Adding value to aluminosilicate solid wastes to produce adsorbents, catalysts and filtration membranes for water and wastewater treatment. J Mater Sci 2021;56:1039–63. https://doi.org/10.1007/s10853-020-05276-0.

[3] O'Connor SJ, MacKenzie KJD, Smith ME, Hanna JV. Ion exchange in the charge-balancing sites of aluminosilicate inorganic polymers. J Mater Chem 2010;20:10234. https://doi.org/10.1039/c0jm01254h.

[4] Novais RM, Gameiro T, Carvalheiras J, Seabra MP, Tarelho LAC, Labrincha JA, et al. High pH buffer capacity biomass fly ash-based geopolymer spheres to boost methane yield in anaerobic digestion. J Clean Prod 2018;178:258–67. https://doi.org/10.1016/j.jclepro.2018.01.033.

[5] Zhang C, Su H, Baeyens J, Tan T. Reviewing the anaerobic digestion of food waste for biogas production. Renew Sustain Energy Rev 2014;38:383–92. https://doi.org/10.1016/j.rser.2014.05.038.

[6] Gonçalves NPF, Da Silva EF, Tarelho LAC, Labrincha JA, Novais RM. Simultaneous removal of multiple metal(loid)s and neutralization of acid mine drainage using 3D-printed bauxite-containing geopolymers. J Hazard Mater 2024;462:132718. https://doi.org/10.1016/j.jhazmat.2023.132718.

[7] Wacławek S, Lutze HV, Sharma VK, Xiao R, Dionysiou DD. Revisit the alkaline activation of peroxydisulfate and peroxymonosulfate. Curr Opin Chem Eng 2022;37:100854. https://doi.org/10.1016/j.coche.2022.100854.

[8] Lee J, Von Gunten U, Kim J-H. Persulfate-Based Advanced Oxidation: Critical Assessment of Opportunities and Roadblocks. Environ Sci Technol 2020;54:3064–81. https://doi.org/10.1021/acs.est.9b07082.

[9] Wang J, Wang S. Activation of persulfate (PS) and peroxymonosulfate (PMS) and application for the degradation of emerging contaminants. Chem Eng J 2018;334:1502–17. https://doi.org/10.1016/j.cej.2017.11.059.

[10] Criquet J, Leitner NKV. Degradation of acetic acid with sulfate radical generated by persulfate ions photolysis. Chemosphere 2009;77:194–200. https://doi.org/10.1016/j.chemosphere.2009.07.040.

[11] Liang C, Su H-W. Identification of Sulfate and Hydroxyl Radicals in Thermally Activated Persulfate. Ind Eng Chem Res 2009;48:5558–62. https://doi.org/10.1021/ie9002848.

[12] Qi C, Liu X, Ma J, Lin C, Li X, Zhang H. Activation of peroxymonosulfate by base: Implications for the degradation of organic pollutants. Chemosphere 2016;151:280–8. https://doi.org/10.1016/j.chemosphere.2016.02.089.

[13] Furman OS, Teel AL, Watts RJ. Mechanism of base activation of persulfate. Environ Sci Technol 2010;44:6423–8. https://doi.org/10.1021/es1013714.

[14] Adam W, Kazakov DV, Kazakov VP. Singlet-oxygen chemiluminescence in peroxide reactions. Chem Rev 2005;105:3371–87. https://doi.org/10.1021/cr0300035.

[15] Oh W-D, Dong Z, Lim T-T. Generation of sulfate radical through heterogeneous catalysis for organic contaminants removal: current development, challenges and prospects. Appl Catal B Environ 2016;194:169–201. https://doi.org/10.1016/j.apcatb.2016.04.003.

[16] Anipsitakis GP, Dionysiou DD. Radical generation by the interaction of transition metals with common oxidants. Environ Sci Technol 2004;38:3705–12. https://doi.org/10.1021/es035121o.

[17] Directive (EU) 2024/3019 of the European Parliament and of the Council of 27 November 2024 concerning urban wastewater treatment (recast) (Text with EEA relevance), (n.d.).

[18] Kosek K, Luczkiewicz A, Fudala-Książek S, Jankowska K, Szopińska M, Svahn O, et al. Implementation of advanced micropollutants removal technologies in wastewater treatment plants (WWTPs) - Examples and challenges based on selected EU countries. Environ Sci & Policy 2020;112:213–26. https://doi.org/10.1016/j.envsci.2020.06.011.

[19] P. Wunderlin, S. Bitterwolf, Micropollutant elimination in Swiss wastewater treatment plants: Experiences and developments, Swiss Association Waste water and Water protection professionals, Glattbrugg, Switzerland, 2025. ⟨https://micropoll.ch/wp-content/uploads/2025/05/20250502_Micropollutant-Elimination-in-Switzerland.pdf⟩.

[20] Zhou Y, Jiang J, Gao Y, Pang S-Y, Ma J, Duan J, et al. Oxidation of steroid estrogens by peroxymonosulfate (PMS) and effect of bromide and chloride ions: Kinetics, products, and modeling. Water Res 2018;138:56–66. https://doi.org/10.1016/j.watres.2018.03.045.

[21] Li C-X, Chen C-B, Wang Y-J, Fu X-Z, Cui S, Lu J-Y, et al. Insights on the pH-dependent roles of peroxymonosulfate and chlorine ions in phenol oxidative transformation. Chem Eng J 2019;362:570–5. https://doi.org/10.1016/j.cej.2019.01.057.

[22] Rabbil M, Bhuyan M, Alzeer M, Adesanya E, Luukkonen T. Transition metal-modified alkali-activated aluminosilicate foams as catalysts for peracetic acid in phenol abatement. Ceram Int 2025;51:28561–71. https://doi.org/10.1016/j.ceramint.2025.04.065.

[23] Luukkonen T, Von Gunten U. Oxidation of organic micropollutant surrogate functional groups with peracetic acid activated by aqueous Co(II), Cu(II), or Ag(I) and geopolymer-supported Co(II). Water Res 2022;223:118984. https://doi.org/10.1016/j.watres.2022.118984.

[24] Gokulakrishnan S, Mohammed A, Prakash H. Determination of persulphates using N,N-diethyl-p-phenylenediamine as colorimetric reagent: oxidative coloration and degradation of the reagent without bactericidal effect in water. Chem Eng J 2016;286:223–31. https://doi.org/10.1016/j.cej.2015.10.058.

[25] Yang H, Choi G-R, Park S-J, Lee C-G. Selective degradation of phenols/nonphenols via biochar-mediated persulfate activation: influence of redox potential on dominant reactive oxygen species formation. J Water Process Eng 2025;75:108094. https://doi.org/10.1016/j.jwpe.2025.108094.

[26] Wang L, Lan X, Peng W, Wang Z. Uncertainty and misinterpretation over identification, quantification and transformation of reactive species generated in catalytic oxidation processes: A review. J Hazard Mater 2021;408:124436. https://doi.org/10.1016/j.jhazmat.2020.124436.

[27] Gonçalves PJ, Bezzerra FC, Teles AV, Menezes LB, Alves KM, Alonso L, et al. Photoinactivation of Salmonella enterica (serovar Typhimurium) by tetra-cationic porphyrins containing peripheral [Ru(bpy)2Cl]+ units. J Photochem Photobiol A Chem 2020;391:112375. https://doi.org/10.1016/j.jphotochem.2020.112375.

[28] Liu G, Zhao J, Hidaka H. ESR spin-trapping detection of radical intermediates in the TiO2-assisted photo-oxidation of sulforhodamine B under visible irradiation. J Photochem Photobiol A Chem 2000;133:83–8. https://doi.org/10.1016/S1010-6030(00)00227-6.

[29] Sawyer DT, Valentine JS. How super is superoxide? Acc Chem Res 1981;14:393–400. https://doi.org/10.1021/ar00072a005.

[30] Hu J, Zeng X, Yin Y, Liu Y, Li Y, Hu X, et al. Accelerated alkaline activation of peroxydisulfate by reduced rubidium tungstate nanorods for enhanced degradation of bisphenol A. Environ Sci Nano 2020;7:3547–56. https://doi.org/10.1039/D0EN00840K.

[31] Lou X, Fang C, Geng Z, Jin Y, Xiao D, Wang Z, et al. Significantly enhanced base activation of peroxymonosulfate by polyphosphates: kinetics and mechanism. Chemosphere 2017;173:529–34. https://doi.org/10.1016/j.chemosphere.2017.01.093.

[32] Yao Z, Chen R, Han N, Sun H, Wong NH, Ernawati L, et al. Natural manganese ores for efficient removal of organic pollutants via catalytic peroxymonosulfate-based advanced oxidation processes. Asia-Pac J Chem Eng 2023;18:e2907. https://doi.org/10.1002/apj.2907.

[33] Qi C, Liu X, Ma J, Lin C, Li X, Zhang H. Activation of peroxymonosulfate by base: Implications for the degradation of organic pollutants. Chemosphere 2016;151:280–8. https://doi.org/10.1016/j.chemosphere.2016.02.089.

[34] Wu L, Lin Y, Zhang Y, Wang P, Ding M, Nie M, et al. $Ca(OH)_2$ -mediated activation of peroxymonosulfate for the degradation of bisphenol S. RSC Adv 2021;11:33626–36. https://doi.org/10.1039/D1RA05286A.

[35] Guan Y-H, Ma J, Li X-C, Fang J-Y, Chen L-W. Influence of pH on the Formation of Sulfate and Hydroxyl Radicals in the UV/Peroxymonosulfate System. Environ Sci Technol 2011;45:9308–14. https://doi.org/10.1021/es2017363.

[36] Liao Z, Zhu J, Jawad A, Muzi J, Chen Z, Chen Z. Degradation of Phenol Using Peroxymonosulfate Activated by a High Efficiency and Stable CoMgAl-LDH Catalyst. Materials 2019;12:968. https://doi.org/10.3390/ma12060968.

[37] Rabbil M, Bhuyan M, Alzeer M, Adesanya E, Luukkonen T. Transition metal-modified alkali-activated aluminosilicate foams as catalysts for peracetic acid in phenol abatement. Ceram Int 2025;51:28561–71. https://doi.org/10.1016/j.ceramint.2025.04.065.

[38] Luukkonen T, Bhuyan M, Hokajärvi A-M, Pitkänen T, Miettinen IT. Water disinfection with geopolymer–bentonite composite foam containing silver nanoparticles. Mater Lett 2022;311:131636. https://doi.org/10.1016/j.matlet.2021.131636.

[39] Zhao X, Jia X, Li H, Zhang H, Zhou X, Zhou Y, et al. Efficient degradation of Health-threatening organic pollutants in water by atomically dispersed Cobalt-Activated peroxymonosulfate. Chem Eng J 2022;450:138098. https://doi.org/10.1016/j.cej.2022.138098.
[40] Chen L, Duan J, Du P, Sun W, Lai B, Liu W. Accurate identification of radicals by in-situ electron paramagnetic resonance in ultraviolet-based homogenous advanced oxidation processes. Water Res 2022;221:118747. https://doi.org/10.1016/j.watres.2022.118747.
[41] Wang N, Lin C, Ren Z, Xu Q, Wang S. Radical and non-radical mechanisms for removal of micropollutants in peroxymonosulfate activation systems: Their generation and identification. Appl Catal B Environ Energy 2026;383:126139. https://doi.org/10.1016/j.apcatb.2025.126139.
[42] Manickavasagam G, Bao W, He C, Zhou T, Oh W-D. Chemical scavengers as probes for mechanistic elucidation in persulfate-based advanced oxidation processes: Insights into their accuracy and reliability. Sep Purif Technol 2026;393:137193. https://doi.org/10.1016/j.seppur.2026.137193.
[43] Manickavasagam G, Bao W, He C, Zhou T, Oh W-D. Chemical scavengers as probes for mechanistic elucidation in persulfate-based advanced oxidation processes: insights into their accuracy and reliability. Sep Purif Technol 2026;393:137193. https://doi.org/10.1016/j.seppur.2026.137193.
[44] Lee J, Von Gunten U, Kim J-H. Persulfate-based advanced oxidation: critical assessment of opportunities and roadblocks. Environ Sci Technol 2020;54:3064–81. https://doi.org/10.1021/acs.est.9b07082.
[45] Lin Z, Du Q, Pei L, Jiang X, Liu S, Xie M, et al. Unraveling the underlying contribution of 1O2 to pollutant degradation during peroxymonosulfate activation by chloride. Appl Catal B Environ Energy 2025;376:125446. https://doi.org/10.1016/j.apcatb.2025.125446.
[46] Cheng K, Zhang L, McKay G. Evaluating the microheterogeneous distribution of photochemically generated singlet oxygen using furfuryl amine. Environ Sci Technol 2023;57:7568–77. https://doi.org/10.1021/acs.est.3c01726.
[47] Chen H, Lin T, Wang P, Wang Y, Wei W, Zhu S. A novel solar-activated chlorine dioxide process for atrazine degradation in drinking water. Water Res 2023;239:120056. https://doi.org/10.1016/j.watres.2023.120056.
[48] Buxton GV, Greenstock CL, Helman WP, Ross AB. Critical review of rate constants for reactions of hydrated electrons, hydrogen atoms and hydroxyl radicals (·OH/·O− in Aqueous Solution. J Phys Chem Ref Data 1988;17:513–886. https://doi.org/10.1063/1.555805.
[49] Clifton CL, Huie RE. Rate constants for hydrogen abstraction reactions of the sulfate radical, $SO_4^{\cdot-}$. Alcohols. Int J Chem Kinet 1989;21:677–87. https://doi.org/10.1002/kin.550210807.
[50] Rodgers MAJ. Solvent-induced deactivation of singlet oxygen: additivity relationships in nonaromatic solvents. J Am Chem Soc 1983;105:6201–5. https://doi.org/10.1021/ja00358a001.
[51] Gao L, Guo Y, Zhan J, Yu G, Wang Y. Assessment of the validity of the quenching method for evaluating the role of reactive species in pollutant abatement during the persulfate-based process. Water Res 2022;221:118730. https://doi.org/10.1016/j.watres.2022.118730.
[52] Haag WR, Hoigné J, Gassman E, Braun A. Singlet oxygen in surface waters — Part I: Furfuryl alcohol as a trapping agent. Chemosphere 1984;13:631–40. https://doi.org/10.1016/0045-6535(84)90199-1.
[53] Zhao X, Li X, Zhu Z, Hu W, Zhang H, Xu J, et al. Single-atom Co embedded in BCN matrix to achieve 100% conversion of peroxymonosulfate into singlet oxygen. Appl Catal B Environ 2022;300:120759. https://doi.org/10.1016/j.apcatb.2021.120759.
[54] Zhao H, Peng J, Chen Z, Zhou Y, Xu M, Zhang H, et al. Curvature strain tunes electron transfer accelerates peroxymonosulfate activation to achieve high-efficiency advanced oxidation. Chem Eng J 2024;497:154831. https://doi.org/10.1016/j.cej.2024.154831.
[55] Wei Z, Villamena FA, Weavers LK. Kinetics and mechanism of ultrasonic activation of persulfate: an in situ EPR spin trapping study. Environ Sci Technol 2017;51:3410–7. https://doi.org/10.1021/acs.est.6b05392.
[56] Bai S, Wang P, Xu C, Wang L, Hu X, Hu P, et al. Dimethyl sulfoxide as a qualitative EPR indicator of sulfate radical in advanced oxidation processes. Water Res 2026;289:125011. https://doi.org/10.1016/j.watres.2025.125011.
[57] Buettner GR. Spin Trapping: ESR parameters of spin adducts 1474 1528V. Free Radic Biol Med 1987;3:259–303. https://doi.org/10.1016/S0891-5849(87)80033-3.
[58] Tai C, Peng J-F, Liu J-F, Jiang G-B, Zou H. Determination of hydroxyl radicals in advanced oxidation processes with dimethyl sulfoxide trapping and liquid chromatography. Anal Chim Acta 2004;527:73–80. https://doi.org/10.1016/j.aca.2004.08.019.
[59] Wen Y, Huang C-H, Ashley DC, Meyerstein D, Dionysiou DD, Sharma VK, et al. Visible light-induced catalyst-free activation of peroxydisulfate: pollutant-dependent production of reactive species. Environ Sci Technol 2022;56:2626–36. https://doi.org/10.1021/acs.est.1c06696.
[60] Wen Y, Huang C-H, Ashley DC, Meyerstein D, Dionysiou DD, Sharma VK, et al. Visible light-induced catalyst-free activation of peroxydisulfate: pollutant-dependent production of reactive species. Environ Sci Technol 2022;56:2626–36. https://doi.org/10.1021/acs.est.1c06696.